Simulation aided design of a low cost ion mobility spectrometer based on printed circuit boards

Abstract

Miniaturized low-cost drift tubes with high analytical performance are a key component for the design of powerful and mass-deployable hand-held ion mobility spectrometers. Thus, a simple model that estimates the influence of the geometrical dimensions on the analytical performance is highly desirable for an effective design process. In this work, we present a simple procedure to predict peak distortion based on only the electrical field distribution inside the drift tube, which can be rapidly simulated using the finite element method. A simulation of the ion motion is not required. Based on these results, we developed an ion mobility spectrometer manufactured entirely from standard printed circuit boards (PCB). Since no additional components were used apart from electrical and gas connectors, ion source and metal grids, the presented ion mobility spectrometer is very simple and inexpensive. Nevertheless, the design provides a resolving power of 82 at a drift length of 50 mm and a drift voltage of 3 kV using a tritium ion source and a field switching shutter. The limits of detection for one second of averaging are 80 ppt_v for acetone, 35 ppt_v for dimethyl methylphosphonate and 180 ppt_v for methyl salicylate.

Introduction

An ion mobility spectrometer (IMS) is a device for detecting trace gases in air originally developed for detection of explosives and drugs [1]. Within the last decade, IMS entered new markets, for example in medical applications [2; 3] or as detectors for chemicals in industrial environments [4]. To reach an even wider field of possible applications, many research groups are working on new techniques to improve the performance of IMS. However, to push IMS in the mass-deployable hand-held sector, the main focus are basically low prices and a compact and robust design. Therefore, we developed a design which is suitable for low cost and portable applications while maintaining the resolving power of laboratory-grade systems.

The ion separation in a drift tube IMS is the result of ion motion along the axis of the drift tube driven by a homogeneous electrical field. To initiate the measurement, a packet of ions is injected into the drift tube. During their motion, the ions are separated based on their mobility in the present drift gas. At the end of the drift tube, the ions are captured by a detector which converts and amplifies the ion current into a measurable voltage. By plotting the measured voltage over the drift time, i.e. the time the ions need to reach the detector, a spectrum is obtained. Without interferences, each ion species will create a Gaussian shaped peak in the spectrum, which can be used to identify the components of the ionized gas.

Two important parameters which characterize the performance of an IMS are the resolving power (R_p) and the limits of detection (LOD). The resolving power is defined as the quotient of the drift time t_d and the full width at half maximum (w_{FWHM}) of the corresponding Gaussian peak in the spectrum.

$$R_p = \frac{t_d}{w_{FWHM}} \quad (1)$$

Therefore, it is a measure for the ability to separate substances with similar mobilities. A low resolving power might lead to a spectrum with overlapping peaks, while a high resolving power yields a clear separation of all visible components. The limit of detection refers to the systems capability to detect a given substance. Typically, the LOD is defined as the concentration generating a signal amplitude equal to three times the standard deviation of the noise. Thus, a large signal-to-noise-ratio (SNR) is essential for achieving good limits of detection.

Simulation based design process

A typical drift tube IMS basically consists of three parts - the ion source, the drift tube and the detector. Of these components, the drift tube typically is the largest, includes the highest number of components and therefore most likely provides the highest optimization potential.

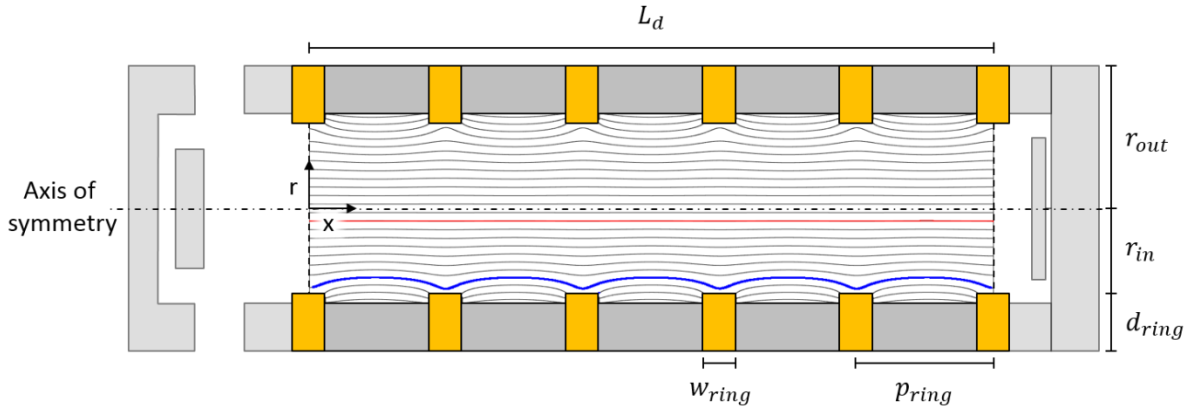

Figure 1: Distribution of the electrical field $E_{(x,r)}$ in a simplified geometrical model. The length of the drift tube L_d is determined by the number of rings n_{ring} and the pitch p_{ring} between two guard ring centers. The outer radius of the tube r_{out} is given by the ring depth d_{ring} and the inner radius r_{in}.

The required space for the drift tube is determined by its length L_d and its outer radius r_{out}. Since the systems resolving power is determined by the length L_d and the peak width due to injection w_{inj} and amplifier w_{amp} as shown in eq. (2), we cannot reduce the length without improving the ion shutter and amplifier if a constant resolving power is required [5].

$$R_p \sim \sqrt[3]{\frac{L_d^2}{\sqrt{w_{inj}^2 + w_{amp}^2}}} \qquad (2)$$

However, there is no immediate impact of the outer radius r_{out} on the resolving power. Nevertheless, a homogenous electrical field is imperative for maintaining IMS resolving power, thus creating an indirect influence of the outer radius on the resolving power. Therefore, it is necessary to analyze the relationships between r_{out} and the electrical field distribution $E_{(x,r)}$, which is illustrated inside the drift tube in Figure 1. While the field is homogeneous on the axis of symmetry marked by the dashed line, distortions arise near the electrodes due to the constant electrical potential on a drift ring. As the ion trajectories will follow the streamlines of the electrical field due to the constant collisions with the drift gas, ions far from the axis of symmetry will take a longer, curved path (blue line) compared to the

trajectories close to the axis (red line). Thus, the drift time of an ion depends not only on its mobility, but also on its radial position inside the drift tube, which can lead to ions with the same mobility arriving at different drift times [6]. As this phenomenon only causes delay, it leads to peak tailing and may reduce the analytical power of the drift tube due to broader and therefore lower peaks. A common method to ensure a clear Gaussian peak shape in the presence of field distortions is masking ions traveling far from the axis of symmetry. Unfortunately, this will lead to a lower signal amplitude and therefore a lower SNR.

Numerical Field Simulations

To generalize the simulations, the radius *r* measured from the axis of symmetry as shown in Figure 1 will be described in terms of the normalized radius *Γ*, where *Γ* is given by the radius *r* divided by the inner tube radius r_{in}.

$$\Gamma = \frac{r}{r_{in}} \tag{3}$$

To begin with, it is necessary to determine the relationship between ring dimensions and peak shape. To do so, the ion distribution on the detector plane was calculated by simulating the ion trajectories in a given field distribution employing *COMSOL Multiphysics* using the *Transport of Diluted Species* module. The generated data can be used to evaluate the time related ion flux at each point of the detector in terms of the normalized radius *Γ*.

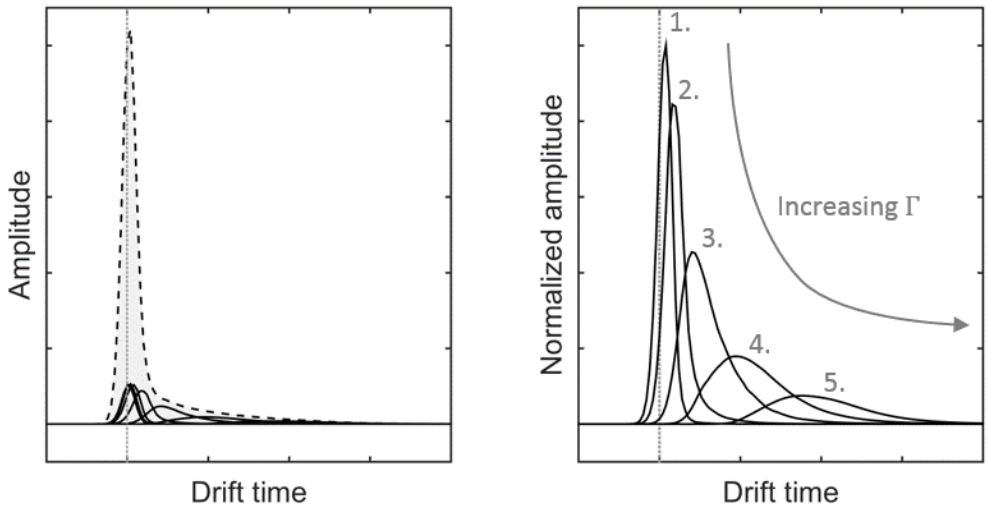

Figure 2: On the left half, a simulation of the signal (dashed) resulting from distorted and delayed ion plugs (solid lines) reaching the detector is shown. On the right half, an enlargement of the peaks corresponding to the five most distorted ion plugs is shown. The data are generated by solving the ion motion in the field distribution presented in Figure 1.

Simulating the ion trajectories in an electrical field as the one shown in Figure 1 a peak shape as illustrated by the dashed line on the left half of Figure 2 can be obtained. Dividing this integrated signal into a number of discrete ion plugs (solid lines) moving on different normalized radiuses *Γ* allows a detailed analysis of the relationship between the distribution of the electrically field and the overall peak shape.

As illustrated in the right half of Figure 2, ion plugs closer to the axis of symmetry (1.) are nearly Gaussian shaped, while plugs moving close to the electrodes are delayed and asymmetrically broadened (5.). As most ion plugs move in a homogenous field, the integrated signal shown in the left half of Figure 2 is similar to a Gaussian peak with the expected drift time (dotted line), but reveals a small tailing. Thus, we define an effective radius Γ_{eff} including all trajectories without significant negative impact on the peak shape. Γ_{eff} therefore describes the effective usable radius of the drift tube.

To decide which of the illustrated ion plugs can be included without deforming the integrated peak, a mathematical measure for peak deformation is required. The resolving power R_p might be the obvious candidate, as it is the most common criterion for the analytical performance of IMS and is also easy to measure. However, as it is based on the full width at half maximum, it will be insensitive to tailing which occurs far below the half height of the peak, such as the distortion shown on the left hand side of Figure 2. To circumvent this problem, we propose the ideality factor η as the peak height h_{peak} divided by the peak area A_{peak} as given by Eq. (4).

$$\eta = \frac{h_{peak}}{A_{peak}} \qquad (4)$$

As every kind of peak broadening, no matter its shape, must lead to a reduction of peak height at a given peak area, the ideality factor η can be expected to react much more sensitively to the peak tailing shown in Figure 2. Normalization yields an ideality factor which is 1 for the Gaussian shaped peaks moving on the axis of symmetry and < 1 for deformed peaks. For example, on the right hand side of Figure 2, the normalized values of η would be 0.97 for peak 1 and 0.18 for peak 5. The respective normalized resolving power would be 0.95 and 0.20. However, when analyzing the resulting peak shown on the left hand side of Figure 2, the normalized ideality factor is 0.71, while the normalized resolving power remains at 0.95. Thus, only the ideality provides a useful mathematical measure for peak deformation in this case.

Unfortunately, calculating either η or R_p requires numerical simulations of ion trajectories, which are much more time consuming than the calculation of the electrical field, as they must be solved for every time step of the simulation instead of only once. Thus, a parameter sweep sufficiently resolved for drift tube development would consume too much time to be feasible. Therefore, we propose a third method, which provides an approximation based on only the electrical field distribution $E_{(x,r)}$, which can be simulated within seconds or minutes. It is based on a two-step approach:

First, the peak position is calculated as a function of Γ. To do so, the inverse of the axial component of the electrical field multiplied by the inverse mobility K is integrated along the length of the drift tube at the given Γ, which serves as a measure for the drift time along this line.

$$\Delta t_{d_{(\Gamma)}} = \int_0^{L_d} \frac{1}{E_{(x,\Gamma)} \cdot K}\, dx \qquad (5)$$

This value is then normalized to the result at $\Gamma = 0$, which is just the length of the drift tube L_d squared divided by the drift voltage U_d due to the homogenous field at this position.

$$t_d = \frac{{L_d}^2}{U_d \cdot K} \tag{6}$$

The result is a measure for the delay of the peak at the given Γ compared to its ideal drift time t_d.

$$\frac{\Delta t_{d_{(\Gamma)}}}{t_d} = \int_0^{L_d} \frac{U_d}{E_{(x,\Gamma)} \cdot {L_d}^2}\, dx \tag{7}$$

Secondly, the radial component of the electrical field is evaluated as a measure for the interaction of peaks at different Γ. To do so, the radial electrical field distribution is integrated similarly to the method presented in eq. (7). The resulting voltage can be used to estimate the radial ion motion leading to interferences between ion plugs moving next to each other. Furthermore, by taking into account the radial diffusion, the estimation of the peak overlap can be improved even further. By using the drift times calculated with eq. (7) and assuming ideal Gaussian peaks only broadened by the additional diffusion due to the extra drift time, the resulting peak shape only gives a rough approximation of the reality (Figure 3, top). By considering the field driven and diffusive radial ion motion, the ion plugs become additionally broadened and slightly shifted (Figure 3, middle), which allows a much better approximation of the ion distribution obtained from an ion motion simulation (Figure 3, bottom). The integrated signals in Figure 3 (middle, bottom) are calculated using all evaluated ion plugs, not only the four shown in the picture for clarity.

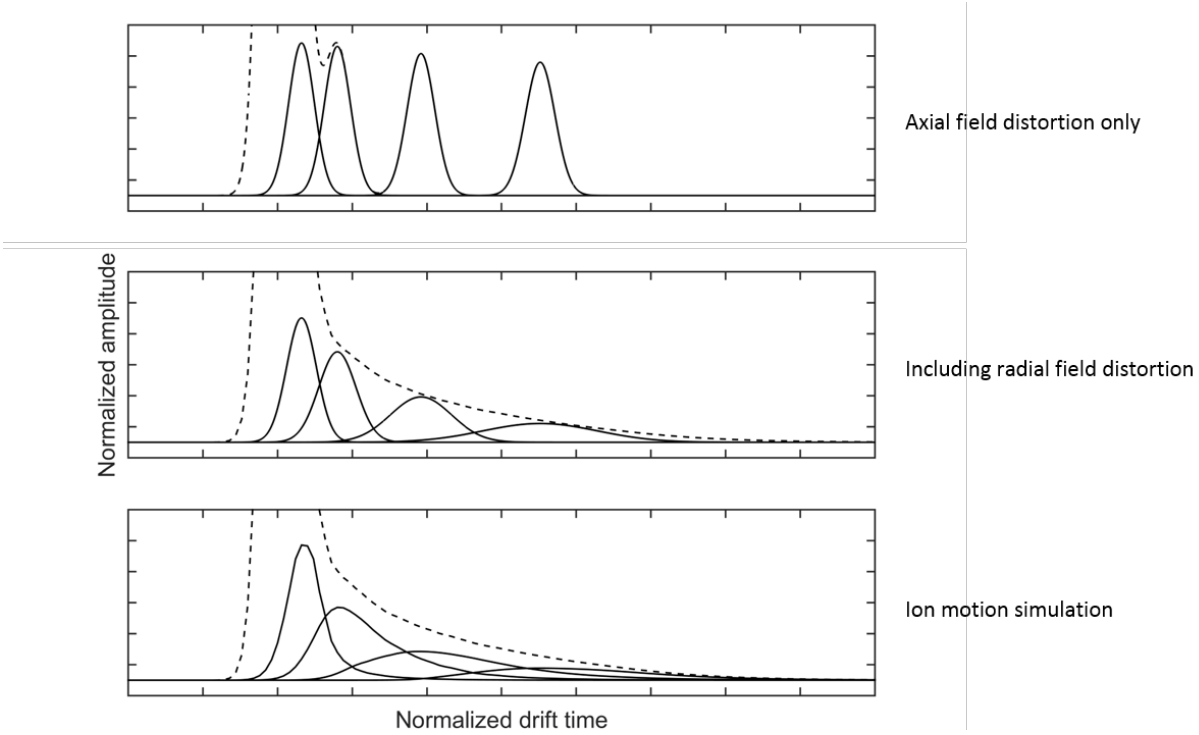

Figure 3: In the first panel, the ion distribution calculated by using only the axial distribution of the electrical field is shown. In the middle, the correction for the radial ion motion is included. The last panel shows the accurately computed ion distribution for comparison.

These three measures for peak deformation are compared in Figure 4. As expected, the resolving power is too optimistic and even predicts no increasing deformation for very high Γ. The approximation from the electrical field only is on the other hand too pessimistic, but follows the ideality factor better in the regions of increasing deformation. Due to its vastly lower computational effort, it will be used for further analysis. The effectively usable radius Γ_{eff} is defined as the value of Γ with the strongest curvature, as it marks the bend in all three curves. The curvature is the highest 2nd derivative, which is determined using a 3rd order Savitzky-Golay-Filter.

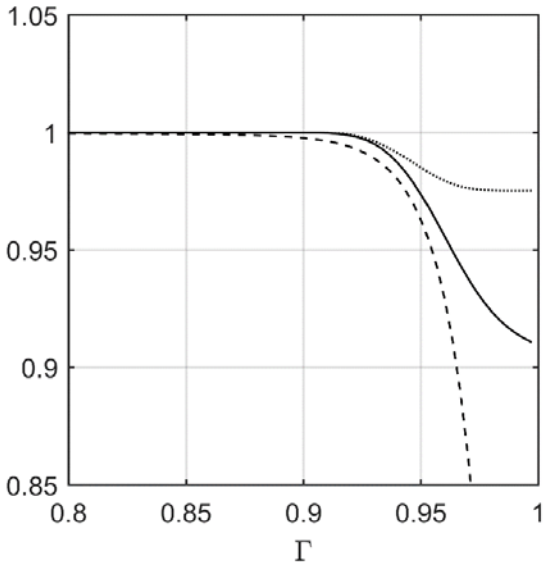

Figure 4: Normalized resolving power (dotted), ideality factor (solid) and electrical field approximation (dashed) as a function of the normalized radius Γ.

Optimized Drift Ring Geometries

It is now possible to compute the electrical field distribution for a number of different geometries with a 2D Field solver and evaluate the results by calculating the effective radius Γ_{eff}. The simulations were performed using radially symmetric model similar to the one described in [7].

As the first step, the ring width w_{ring} was swept. The ring width is given as the ratio between w_{ring} and the pitch between two rings p_{ring}. Changing the absolute values at a constant ratio would not change the results, as it means just scaling up the design. Therefore, the ratios are the parameters of interest. As mentioned above, the complexity and therefore the cost of an IMS depends on the number of discrete elements. Thus, by maintaining a constant pitch p_{ring} we ensure that the number of rings n_{ring} is constant.

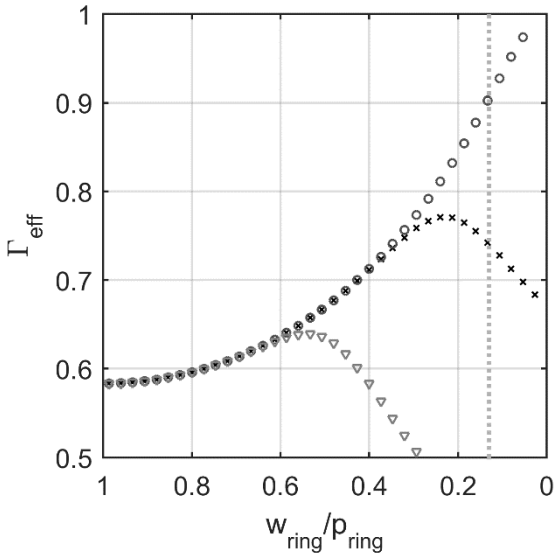

Figure 5: Effectively usable radius Γ_{eff} as a function of w_{ring}/p_{ring} for d_{ring}/p_{ring} = 2 (circle), d_{ring}/p_{ring} = 1 (cross) and d_{ring}/p_{ring} = 0.5 (triangle). The inner tube radius is equal to the pitch (r_{in}/p_{ring} = 1).

As illustrated in Figure 5, decreasing the ring width w_{ring} in relation to p_{ring} will increase the effective useable radius Γ_{eff} up to a certain point. This is expected since a conductive object has a constant electrical potential on its surface and therefor a large w_{ring}/p_{ring} leads to a large potential difference between two rings. Accordingly, the distortion in the electrical field increases with increasing w_{ring}/p_{ring}. Therefore, best results can be achieved by using flat disks as ring geometries which correlates to the results presented by [8]. The main drawback is the missing shielding as shown in Figure 6 due to the poor ratio of ring depth d_{ring} and the gap between two rings. Not only the shape of the drift field is distorted, but also its strength at this position is influenced by the grounded electrodes surrounding the dirft tube.

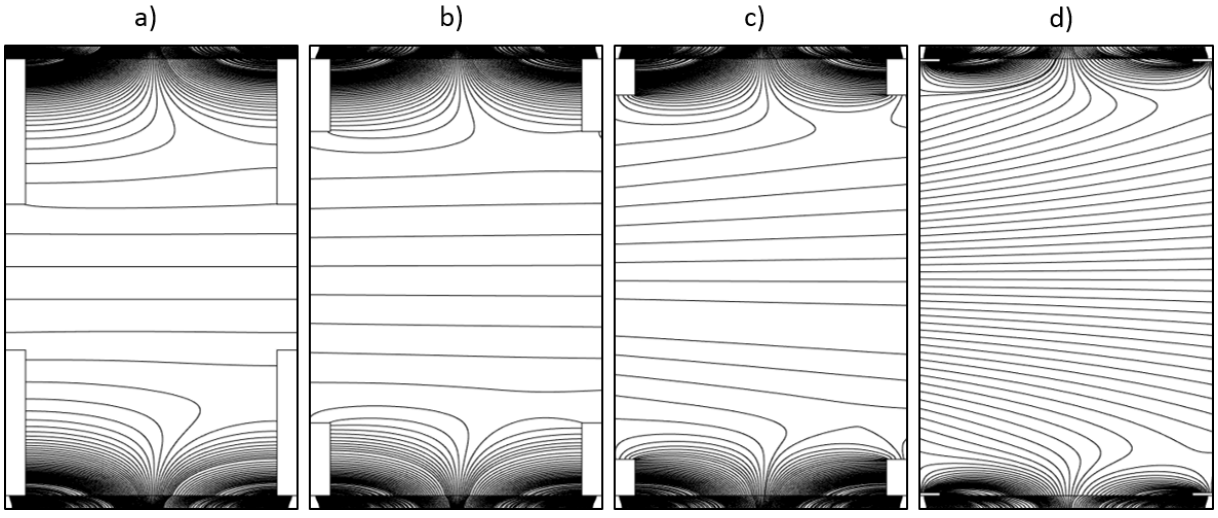

Figure 6: Simulation of the electrical field corresponding to d_{ring}/p_{ring} equal 2, 1, 0.5 and 0.13 (left to right) in presence of a grounded electrode surrounding the drift tube.

This will lead to a decrease of the effectively usable radius Γ_{eff} observed in Figure 5 above a certain w_{ring}/p_{ring}, which depends on the d_{ring}/p_{ring}. Thus, this effect could be overcome by raising the ring depth d_{ring} with decreasing w_{ring}. Nevertheless, in order to achieve an effectively usable radius Γ_{eff} of more than 0.9, a ring depth equal to twice the tube radius r_{in} (Figure 5, circles) would be needed. Therefore, at a constant number of drift rings building a compact IMS is not feasible, as wide rings require a large inner radius and thin rings require either also a large inner radius or a large ring depth. However, increasing the ring depth is only necessary to improve the shielding, which can also be achieved by decreasing the ring pitch p_{ring} at the cost of increasing the number of rings n_{ring} as shown in Figure 7. At a constant ring width w_{ring} and depth d_{ring}, the pitch p_{ring} was swept.

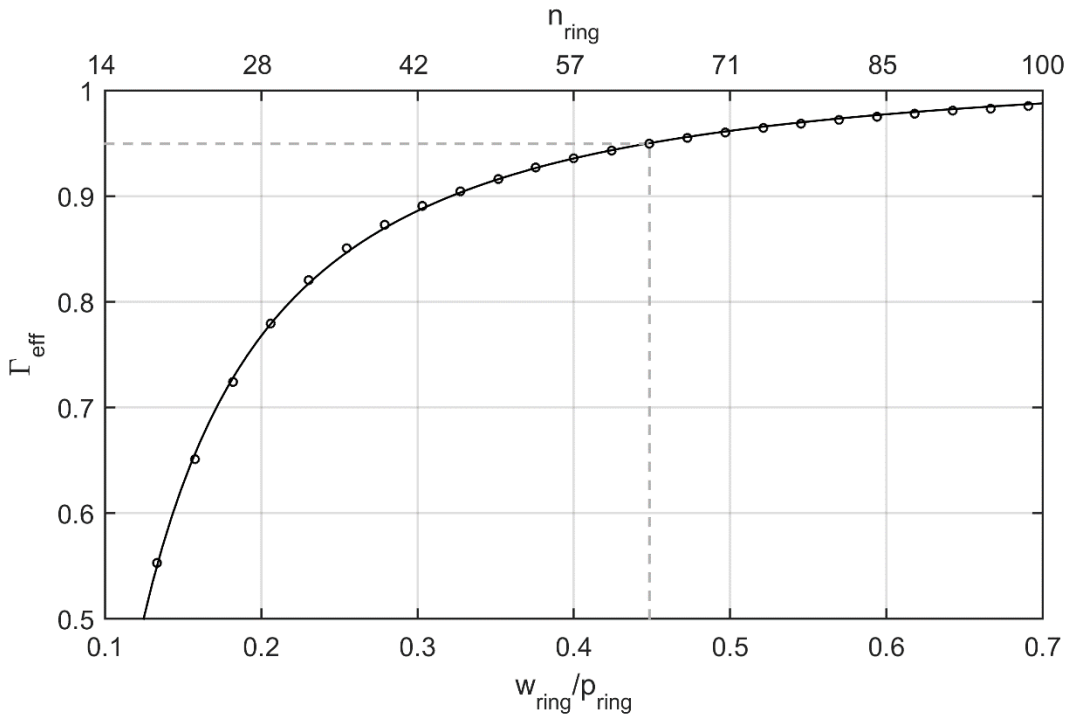

Figure 7: Effectively usable tube radius Γ_{eff} (circles) as a function of w_{ring}/p_{ring} (r_{in}/w_{ring} = 7.5, d_{ring}/w_{ring} = 0.1) and fit with a $x^{(3/2)}$ function (line). The second x-axis shows the number of rings n_{ring} required in an IMS with a drift length of 100 mm.

The large ratio of inner radius r_{in} to ring width w_{ring} used for the simulation presented in Figure 7 equates w_{ring}/p_{ring} = 0.13 as illustrated by the dotted line in Figure 5. According to Figure 5 the used ratio should provide an extremely homogenous electrical field as long as the drift field distortions induced by the surrounding grounded electrodes can be completely shielded by the drift rings, e.g. with a large ring thickness as illustrated by Figure 5 (circles). However, decreasing the ring thickness will increase the influence of the present ground electrode which will entail a dramatic reduction of the effectively usable radius Γ_{eff} as illustrated in Figure 6 d). By reducing the pitch p_{ring}, the effectively usable radius Γ_{eff} can be increased at a constant outer radius even when a grounded electrode is in existence. Thus, if only a certain Γ_{eff} is required regardless the number of rings, the outer radius can be decreased. However, now a suitable technique for accurately producing an extremely high number of closely spaced thin drift rings is required.

Printed Circuit Board IMS

Well-known approaches for manufacturing drift tubes with high numbers of drift rings are the use of low temperature cofired ceramics (LTCC) [9] or resistive glass tubes (RGT) [10]. Simplified, drift tubes manufactured from LTCCs integrate drift rings and resistors into the housing by coating structured raw ceramics with conductive materials before baking the structure. While the LTCC still relies on discrete rings, the RGT is based on an isolating glass tube completely coated with a resistive material acting as both drift ring and resistor simultaneously. This is the equivalent of an infinite number of infinitely small drift rings. However, both approaches are expensive and inflexible due to the complex fabrication process. Another process, which is also able to produce finely spaced structures, but is already widespread and therefore cheap, is the manufacturing of printed circuit boards (PCB), which are part of virtually every electronic device today. The copper on their surface can be structured using lithographic processes to generate the necessary geometries for electrodes and feedthroughs with extremely high precision. Even though a printed circuit board IMS has been reported [11], this approach has not yet gained wide recognition. One of the main disadvantages of PCB manufacturing is the limitation to flat structures. Due to this, the setup reported in [11] uses only electrodes on the top and the bottom of the drift tube, causing deformations of the electrical field close to the sides.

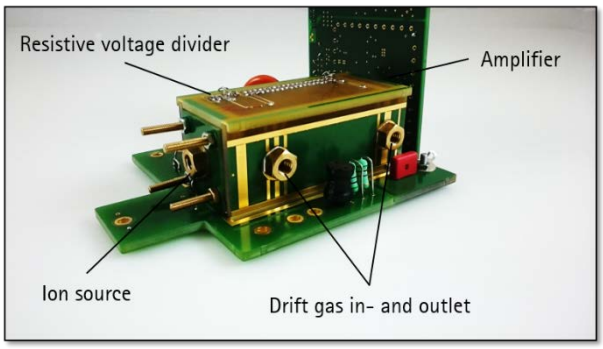

Figure 8: PCB-IMS with the resistive Voltage divider on top, ion source on the left and detector with attached amplifier on the right side.

To overcome this limitation, we developed a drift tube based on the results presented in the simulation section, which is manufactured completely from printed circuit boards. As it incorporates 45 electrodes on each of the four sides of the 50 mm long drift region, it can generate an extremely homogenous drift field while achieving a small size. The used PCBs are made of a glass-reinforced epoxy laminate (FR4) which is laminated with a 35 µm film of copper. The basic layout of the PCB-IMS is similar to a typical stacked ring design, consisting of ionization region, drift region and a detector shielded by an aperture grid. A tritium source is used for ionization and ions are injected into the drift tube using a field switching (FS) shutter [12]. To minimize interferences on the ion signal, the current amplifier is directly attached to the backside of the PCB detector. The epoxy laminate acts as housing, isolator and as substrate for the drift rings simultaneously. The drift rings are connected to a resistive voltage divider placed on the outer layer of the drift tube by vertical interconnections between the inner and outer layers. Purified air is used as both drift gas and sample carrier. The experimental parameters of the setup are summarized in Table 1.

Table 1: Experimental parameters

Parameter	Value	
Drift length	50	mm
Source diameter	10	mm
Source activity	300	MBq
Drift voltage	3150	V
Injection voltage	500	V
Repetition rate	44	Hz
Drift gas flow	500	$mls \cdot min^{-1}$
Sample gas flow	20	$mls \cdot min^{-1}$
Dew point of drift and sample gas	-95.5	°C
	79.4	ppb_v
Operating pressure	1018	mbar
Operating temperature	21	°C

Results and Discussion

In order to analyze the performance of the presented ion mobility spectrometer and to identify the optimal operating point, we measured the resolving power and signal-to-noise-ratio of the positive reactant ion peak as a function of the applied drift voltage. As shown in Figure 9, the resolving power increases with increasing drift voltage up to a maximum at a drift voltage of about 2.9 kV. The signal-to-noise-ratio, normalized to its value at 2.9 kV, increases continuously with increasing drift voltages. Its behavior agrees excellently with the analytical function calculated by [13], which is also shown in Figure 9. Therefore, the operating point is set to 3.2 kV since the loss in resolving power is negligible compared to the increase of the signal-to-noise-ratio.

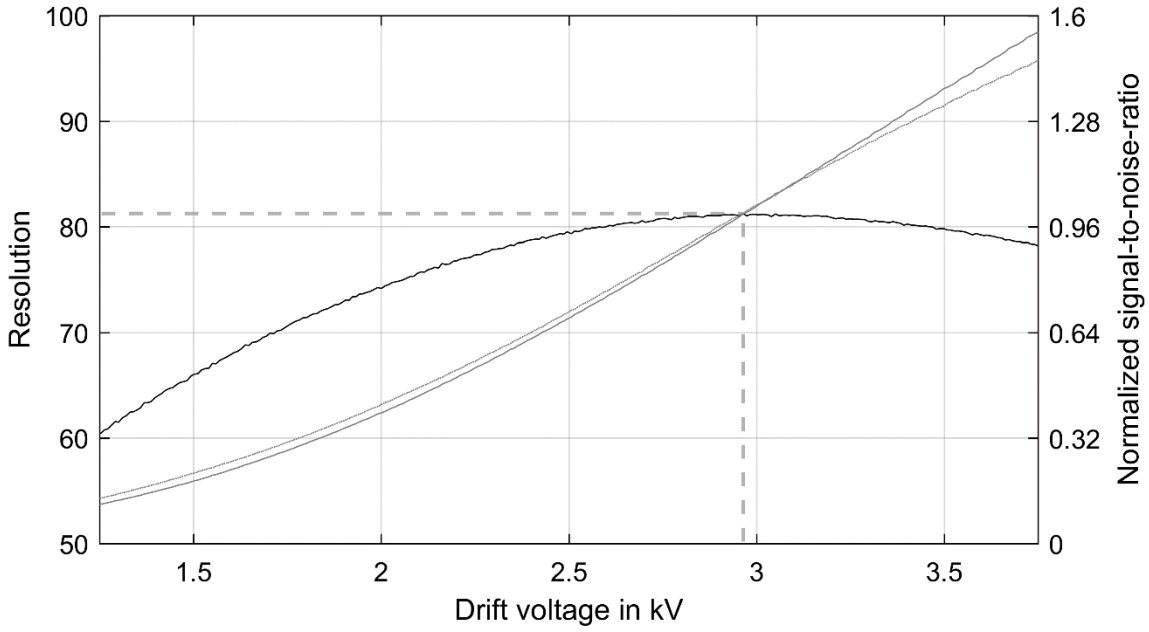

Figure 9: Resolving power (black), normalized measured (gray) and calculated SNR (gray, dotted) with the maximum resolving power of about 82 at a drift voltage of 2.96 kV (dashed lines).

The resulting spectra in both positive and negative mode at a drift voltage of 3.2 kV with 1024 averages are shown in Figure 10. The resolving power of the positive reactant ion peak (RIP^+) is R_p = 82, while the resolving power of the negative reactant ion peak (RIP^-) is R_p = 76. As predicted by the field simulations and the approximation based on it, both peaks are nearly Gaussian shaped without tailing. The lower resolving power of the negative reactant ion peak can be attributed to a second reactant ion species, which is already visible in front of the main peak and can be separated at higher resolving powers [14].

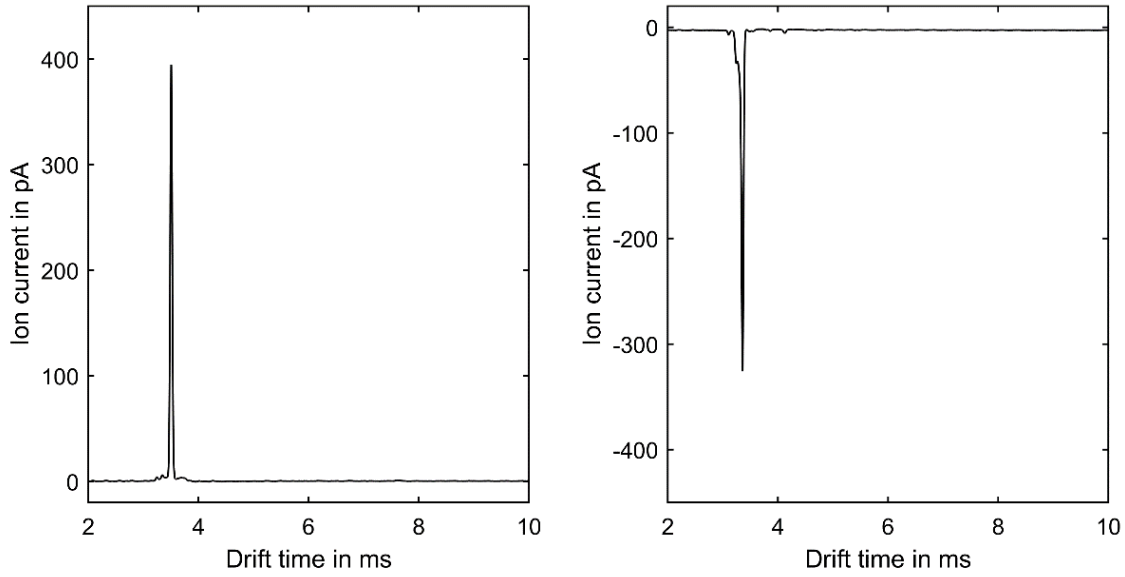

Figure 10: Spectra measured with the PCB-IMS. The positive RIP^+ (left) has a resolving power of R_p = 82, the negative RIP^- (right) a resolving power of R_p = 76.

Figure 11 shows a measurement of 2 ppb_v acetone. The acetone dimer is clearly visible at a normalized drift time of 1.13, while the acetone monomer is only visible as a shoulder of the positive reactant ion peak due to the extremely dry conditions. Again, at higher resolving power, it would become visible [5]. The resulting limit of detection for a measurement time of one second using the acetone dimer is 80 ppt_v. The limit of detection for dimethyl methylphosphonate (DMMP) is 35 ppt_v for the monomer.

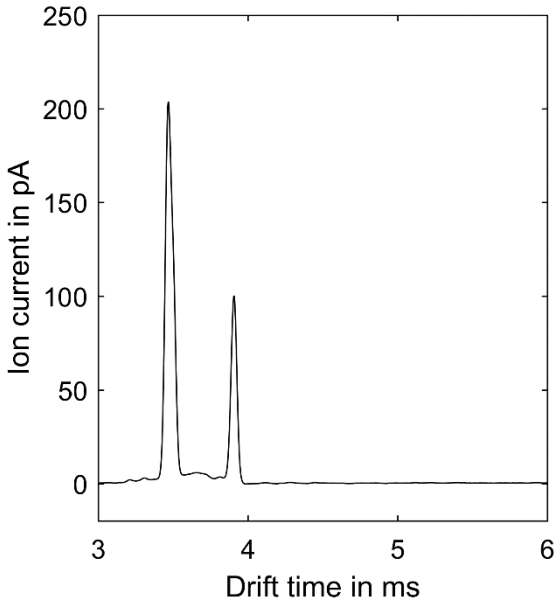

Figure 11: 2 ppb_v acetone 1024 averaged measured with the PCB-IMS.

Figure 12 shows a measurement of 4.3 ppb_v methyl salicylate in the negative mode. Only one product ion peak is formed at a normalized drift time of 1.39. The limit of detection for a measurement time of one second is 180 ppt_v.

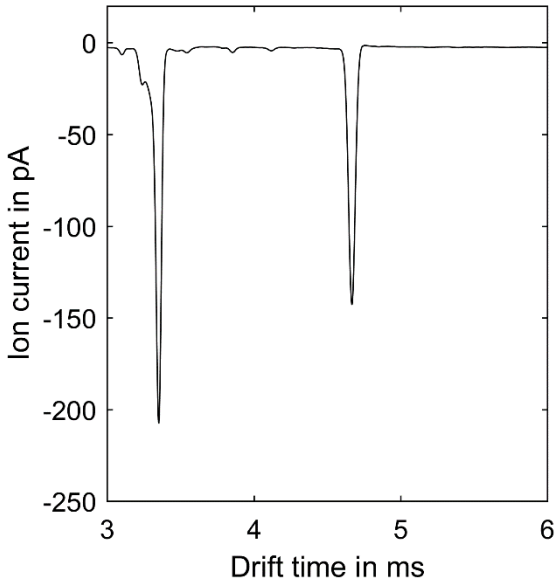

Figure 12: 4.3 ppb_v methyl salicylate measured with the PCB-IMS.

Conclusion

In this work, we presented a method to estimate the influence of the electrical field distribution on the peak shape in a drift tube ion mobility spectrometer using only an electrical field simulation, but no ion motion simulation. All results are given as ratios between the parameters of interest. Therefore, this technique is applicable to any other drift tube design, providing a simple tool for estimating the correct dimensions of a drift cell. Using the developed models, we designed an ion mobility spectrometer based on printed circuit boards only. This device offers a resolving power of about 80 and simultaneously limits of detection for a measurement time of one second in the low ppt_v-range. This demonstrates that low cost, compact, high performance drift tubes are indeed feasible. These could offer a basis for the design of overall low cost ion mobility spectrometer systems with high analytical power, bringing ion mobility spectrometry into more applications.

References

1. Eiceman GA, Karpas Z, Hill HH (2013) Ion mobility spectrometry, 3rd edn. CRC Press, Boca Raton

2. Fink T, Baumbach JI, Kreuer S (2014) Journal of breath research 8:1–11

3. O'Donnell RM, Sun X, Harrington, Peter de B. (2008) TrAC Trends in Analytical Chemistry 27:44–53

4. Borsdorf H, Eiceman GA (2006) Applied Spectroscopy Reviews 41:323–375

5. Kirk AT, Allers M, Cochems P, Langejuergen J, Zimmermann S (2013) The Analyst 138:5200–5207

6. Rokushika S, Hatano H, Baim MA, Hill HH (1985) 57:1902–1907

7. Langejuergen J, Cochems P, Zimmermann S (2012) 15:247–255

8. Soppart O, Baumbach JI (2000) Measurement Science and Technology 11:1473–1479

9. Pfeifer KB, Rumpf AN (2005) 77:5215–5220

10. Kaplan K, Graf S, Tanner C, Gonin M, Fuhrer K, Knochenmuss R, Dwivedi P, Hill HH (2010) Analytical chemistry 82:9336–9343

11. Eiceman GA, Schmidt H, Rodriguez JE, White CR, Krylov EV, Stone JA (2007) Instrumentation Science & Technology 35:365–383

12. Kirk AT, Zimmermann S (2014) International Journal for Ion Mobility Spectrometry 17:131–137

13. Kirk AT, Zimmermann S (2015) International Journal for Ion Mobility Spectrometry 18:129–135

14. Kirk AT, Zimmermann S (2015) International Journal for Ion Mobility Spectrometry 18:17–22